Carpathian Journal of Earth and Environmental Sciences, February 2018, Vol. 13, No. 1, p. 121 – 134; DOI:10.26471/cjees/2018/013/012

ZIRCON U-Pb AGES, GEOCHEMICAL CHARACTERISTICS, Hf ISOTOPE CHARACTERIZATION AND REGIONAL IMPLICATIONS OF THE CHANG7 TUFF IN RUJIGOU AREA, HELAN MOUNTAINS

Yong YANG[1], Kaisheng AN[2], Jiawei CUI[1] & Fei LIU[3]

[1]Institute of Geomechanics, Chinese Academy of Geological Sciences, Beijing, China;
[2]No.5 Oil Production Plant of PetroChina Changqing of Oilfield Company, Xi'an, China;
[3]No.2 Oil Production Plant of PetroChina Changqing of Oilfield Company, Xi'an, China;
**Corresponding author. E-mail address: 1cuijiawei1@163.com*

Abstract: A Chang7 tuff interval (CTR) was found in Rujigou area, Helan Mountains. It is located outside of the range of the Chang7 tuffs in Ordos Basin (CTO) as determined by previous researchers. The aim of this paper is to determine the magmatic origin and tectonic setting of the CTR by analyzing the zircon U-Pb ages, geochemical characteristics and Hf isotope characterization. LA-ICP-MS zircon U-Pb data show CTR crystallized in the 231.2 ± 1.4 Ma. The U-Pb dating results are within the age interval of 242 ~ 205 Ma for the CTO. The CTR and CTO have similar geochemical characteristics and Hf isotope characterization. Therefore, they are the product of volcanic eruption in the same tectonic setting. Due to the wider coverage, the CTR should correspond to the most intense volcanic eruption in the Qinling orogenic belt. A preliminary analysis of the geochemical composition of the CTR suggests a rhyodacite parental magma from volcanic arc-related setting. The volcanic arc setting was related to the subduction of A'nyemaqen–Mianlue Ocean. Geochemical composition suggests Chang 7 tuffs mainly resulted from a partial melting process of lower crustal rocks at depths of 15-35 km. The two-stage Hf-isotope model ages of CTR range from 1.3 Ga to 1.5 Ga. This indicates that the CTR mainly originated from the Mesoproterozoic growth of the crust in the west Qinling orogenic belt.

Key words: Zircon U-Pb age, Geochemistry, Hf isotope, Tuff interval, Yanchang Formation, Helan Mountains

1. INTRODUCTION

Ordos Basin is the second largest sedimentary basin in China, and it is rich in coal, oil, natural gas, uranium ore and other mineral resources (Liu et al., 2006, 2007; Yang & Deng, 2013). The Yanchang Formation in the basin was formed during the maximum development of the intracontinental lacustrine basin. It has always been one of the important formations for oil and gas exploration. Many tuff intervals with different thickness were deposited in the Yanchang Formation. They provide important information for the study of the coupling relationship between the Ordos Basin and the Qinling orogenic belt. Much research has been done on the Chang7 tuff intervals and the main achievements are as follows: (1) The total Chang7 tuffs thickness decreases from southwest to northeast (Fig. 1), indicating that the original volcanic sources must have come from the southwestern part or southern part, out of the present Ordos basin (Deng et al., 2008, 2009, 2013; Qiu et al., 2009, 2010, 2013, 2014); (2) The U-Pb dating of the Chang7 tuffs yielded values within the age interval of 242～205 Ma, with most values concentrated at ～230 Ma (Deng et al., 2008, 2009; Zhang et al., 2009a, 2014; Yang & Deng, 2013; Wang et al., 2014); (3) Most samples fall at the rhyodacite/dacite field on the Zr/TiO2-Nb/Y and TAS magmatic discrimination diagram. It shows that the tuff originated from the neutral to acidic volcanic rocks (Zhang et al., 2009a; Qiu et al., 2011); (4) The two-stage Hf-isotope model ages shows that the Chang7 tuffs mainly originated from Neoproterozoic crustal material. Considering their composition and age, they likely originate from a mixture of Yaolinghe Group basic volcanic rocks and Yunxi Group acid volcanic rocks of South Qinling basement (Zhang et al., 2014).

The Chang7 tuff interval (CTR) was first found

in Rujigou area, Helan Mountains. It is located outside of the range of the Chang7 tuffs in Ordos Basin (CTO). Therefore, further research is needed to determine the affinity between the CTR and CTO. The purpose of this study is to determine the affinity between the two tuff intervals, and to discuss their source and tectonic setting. For this reason, zircon U-Pb ages, geochemical characteristics and Hf isotope characterization of the CTR are analyzed in this paper, and compared with those of the CTO from previously published research.

2. GEOLOGICAL SETTING

Helan Mountains are located in the western part of North China Plate, bounded by the Ordos Block to the east and the Alxa Block to the west (Fig. 1). This area experienced a strong extensional regime in the late Triassic (Liu, 1998; Ritts et al., 2004; Zhao et al., 2007; Liu et al., 2005, 2013; Huang et al., 2015). The sedimentary deposit of the Upper Triassic Yanchang Formation contains sandstones, siltstones, mudstones and tuff intervals with a preserved thickness of about 3000m (Ritts et al., 2004). For exploration and exploitation purposes, the Yanchang Formation in Helan Mountains was informally subdivided into 8 oil reservoir units named Chang8 to Chang1 from the bottom to the top based on marker beds, sedimentary cycles or lithological association (Fig. 2). The Chang7 oil reservoir unit is a deep-water lacustrine deposit, and is composed of carbonaceous and silty shale. A tuff interval was found in Rujigou area, Helan Mountains. Its distribution is relatively uniform, and its thickness is about 0.5 m (Fig. 3a). The tuff is mainly composed of volcanic dust and vitroclastic fragments. The volcanic dust has been converted to chlorite by devitrification, and the vitroclastic fragments have been argillized or replaced by calcite (Fig. 3b).

3. ANALYTICAL METHODS

3.1 Geochemical analysis

To obtain further information regarding the tectonic setting of the volcanic rocks, the elemental contents of the CTR samples were analysed. The samples were oven-dried at 70°C for approximately 24 h and then homogenized; 100 g of each homogenized sample was ground to 200-mesh in an agate mortar for geochemical analyses.

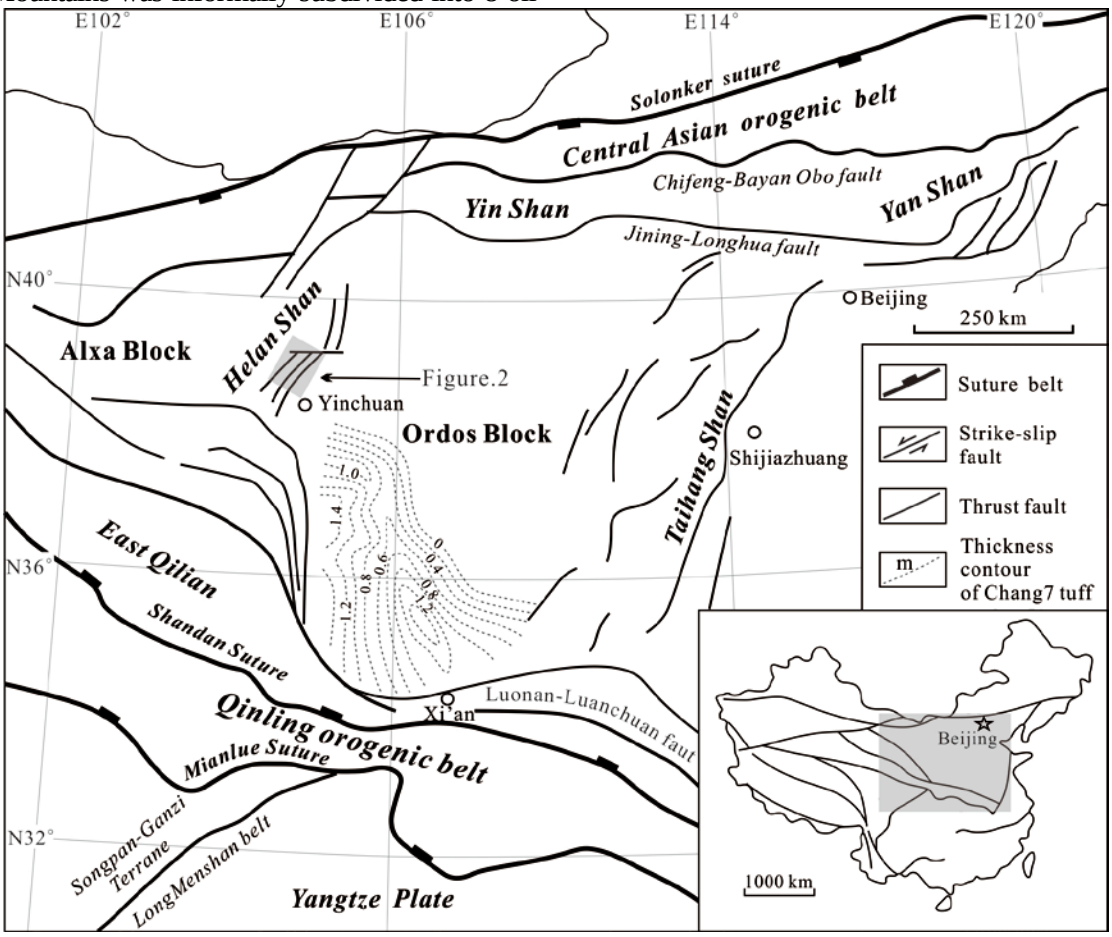

Figure 1. Simplified geological map of the Ordos Basin and its adjacent area (modified from Liu et al., 2013), showing the isopach map (in meters) of the CTO (after Deng et al., 2008, 2009; Qiu et al., 2009, 2014)

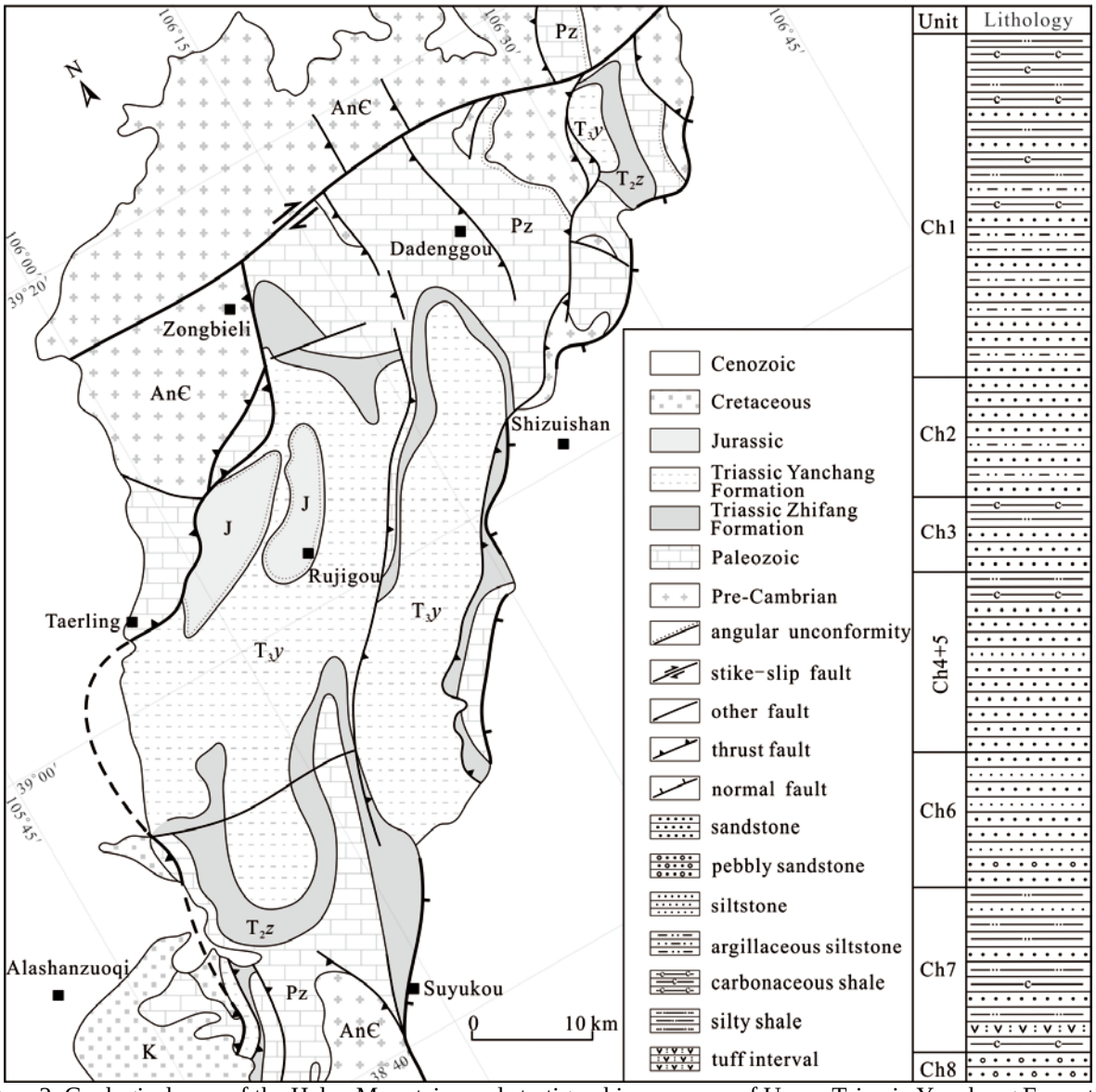

Figure 2. Geological map of the Helan Mountains and stratigraphic sequence of Upper Triassic Yanchang Formation (modified from 1:200,000 geological maps).

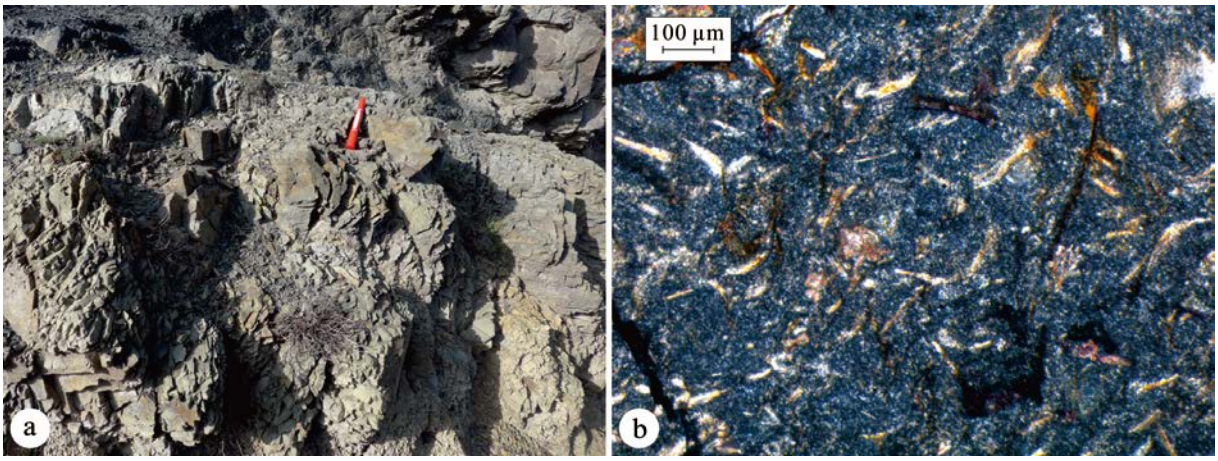

Figure 3. Representative outcrop photo (a) and micrograph (b) of the Chang 7 tuffs in Rujigou area

The elemental analyses were conducted at the National Research Centre for Geoanalysis, China. Details of the analytical methods and apparatus are reported by Li et al., (2014). Measurements of

international standard reference material indicated an analytical precision of 5–10%.

3.2 Zircon U–Pb dating

The U–Pb isotopes of the zircons were determined by an excimer ArF GeoLas 2005 laser ablation system coupled with an Agilent 7500a ICP–MS at the State Key Laboratory of Geological Processes and Mineral Resources, China University of Geosciences, Wuhan, China. Details of the analytical procedures have been described by Liu et al. (2010a, b). The laser beam was typically 32 μm in diameter with a frequency of 6 Hz. Helium was used as the carrier gas to provide efficient aerosol transport to the ICP, and minimize aerosol deposition around the ablation site and within the transport tube (Eggins et al., 1998; Jackson et al., 2004). Nitrogen was added to the central gas flow in the LA–ICP–MS (2 mL min^{-1}) to increase the sensitivity of the U–Th–Pb isotope analysis (Hu et al., 2008). The carrier and make-up gas flows were optimized by ablating NIST SRM 610 to obtain the maximum signal intensity for ^{208}Pb, while keeping ThO/Th and Ca^{2+}/Ca^{+} ratios low, to minimize matrix-induced interferences. Each analysis comprised a background acquisition of 20–30 s (gas blank) followed by 50 s of data acquisition from the sample. Zircon 91500 was used as the external standard for U–Pb dating. Our measurements of GJ-1 yielded weighted average $^{206}Pb/^{238}U$, $^{207}Pb/^{235}U$, and $^{207}Pb/^{206}Pb$ ages of 601.6±1.7Ma (2σ, MSWD=0.41, n=76), 602.9±3.4 Ma (2σ, MSWD=0.32, n=76), and 605±16 Ma (2σ, MSWD=0.30, n=76), respectively, which are within error with the reference age of 599.8 ±1.7 Ma (2σ) (Jackson et al., 2004).

In-house Excel-based software (ICPMSDataCal Ver. 9.0) was used to perform off-line selection and integration of background and analyte signals, for time-drift correction, and quantitative calibration for trace element analysis and U–Pb dating (Liu et al., 2008). Common Pb correction was applied following the method of Andersen (2002). The correction was negligible in most cases. Weighted averages and intercept ages were calculated using ISOPLOT (Ver. 3.76) (Ludwig, 2012).

3.3 Zircon Lu–Hf isotopes

Hf isotope analysis was carried out on a Neptune Plus MC–ICP–MS (Thermo Fisher Scientific, Germany), in combination with the GeoLas 2005 in the State Key Laboratory of Geological Processes and Mineral Resources, China University of Geosciences, Wuhan. Details of the operating conditions for the laser ablation system and the MC–ICP–MS instrument, and data calibration and data processing were reported by Hu et al., (2012). The major limitation to the accurate in situ determination of zircon Hf isotopes by LA–MC–ICP–MS is the very large isobaric interference from ^{176}Yb, and, to a much lesser extent, ^{176}Lu on ^{176}Hf (Woodhead & Hergt, 2010). Interference of ^{176}Lu on ^{176}Hf was corrected by measuring the intensity of the interference-free ^{175}Lu isotope and using the recommended $^{176}Lu/^{175}Lu$ ratio of 0.02656 (Blichert-Toft & Albarède, 1997) to calculate $^{176}Lu/^{177}Hf$ ratios. Similarly, the interference of ^{176}Yb on ^{176}Hf was corrected by measuring the interference-free ^{173}Yb isotope and using the recommended $^{176}Yb/^{173}Yb$ ratio of 0.7962 (Chu et al., 2002) to calculate $^{176}Hf/^{177}Hf$ ratios. The analyses were performed on domains of similar age to the areas used for age determinations, as guided by CL images. Off-line selection and integration of analytical signals, and mass bias calibrations were performed using ICPMSDataCal (Liu et al., 2010a).

The $^{176}Hf/^{177}Hf$ ratios obtained using this technique were 0.2822905±0.0000035 (1σ, MSWD=2.6, n=89) for 91500, and 0.282019±0.000004 (1σ, MSWD=4.5, n=87) for GJ-1. These results are within 2σ of the recommended $^{176}Hf/^{177}Hf$ ratios for 91500 (0.2823075±58, 2σ) (Griffin et al., 2002; Wu et al., 2006) and GJ-1 (0.282015±0.000019, 2σ) (Elhlou et al., 2006).

4. ANALYTICAL RESULTS

4.1 Geochemistry

The chemical compositions of 5 tuff samples were analyzed, with the aims of investigating the tectonic setting of the CTR. The results are shown in Table 1.

4.1.1 Major elements

In the CTR Samples, the SiO_2 content ranges from 74.92 to 76.82, with an average of 75.58 (Table 1), which shows formation from acidic magma. The K_2O + Na_2O content ranges from 2.54 to 2.72 (with an average of 2.64). In the SiO_2 — K_2O + Na_2O diagram, all points are plotted in the rhyolite area (Fig 4). The Al_2O_3 is high (its content ranges from 11.39 to 12.06, with an average of 11.79), with the aluminum index (A/NCK) ranging from 1.24 to 12.06, which suggests that the CTR should be classified as peraluminous volcanic rocks (Fig 5). The contents of FeO, Fe_2O_3, MgO and CaO are relatively low, which is consistent with the evolution trend of the major elements in acidic volcanic rocks. The ratio of TiO_2/Al_2O_3 (weight %) is the most useful indicator for provenance, values less than 0.02 being

typical for acidic volcanic rocks (Zhou et al., 2000; Burger et al., 2002). Our data shows that the TiO_2/Al_2O_3 ratio ranges from 0.005 to 0.007 with an average of 0.0063, which is consistent with an acidic magma origin (Table 1).

4.1.2 Trace elements

Trace element contents of the CTR are also given in Table 1. Total rare earth element (ΣREE) content ranges from 123.57 to 156.28 ppm, with an average of 136.47 ppm, which is higher than the averages of PAAS (182 ppm) (McLennan, 1989) and NASC (176.2 ppm) (Haskin et al., 1968), respectively. The ratio of LREE/HREE (Light REE/Heavy REE) ranges from 5.46 to 5.83 (average 5.66), and the value of (La/Yb)CN (CN = Chondrite Normalized) varies between 4.87 and 5.93 (average 5.47), indicating the CTR are relatively enriched in the LREE. The mean of (La/Sm)CN (2.94) is higher than the average of (Gd/Lu)CN (1.40), suggesting that the LREEs are enriched relative to HREEs. The CTR show a negative Eu anomaly (δEu = 0.19–0.74), indicating plagioclase fractionation. The trends of primitive mantle normalized REE values of the CTR are shown in Fig. 6a, displaying a descending trend of LREE with flat HREE distribution. The evidently negative Eu anomaly and REE distribution pattern suggest the parental magma formed in a subduction-related volcanic arc environment. The CTR show strong positive anomalies of Rb, Th and U and negative anomalies of Nb, Sr and Eu on a spidergram of the primitive mantle normalized values (Fig. 6b), which are thought to be related to a volcanic arc-related setting (Münker, 1998).

Table 1. Major (%) and trace (ppm) element data of the CTR. Note: $\delta Eu = Eu_{CN}/ (SmCN \times Gd_{CN})^{1/2}$; CN = Chondrite Normalized; the normalization value after Sun & McDonough (1989); PREE means total rare earth elements.

Sample	Ru.01	Ru.02	Ru.03	Ru.04	Ru.05	Sample	Ru.01	Ru.02	Ru.03	Ru.04	Ru.05
SiO_2	75.83	75.01	74.92	75.31	76.82	Nb	15.5	14	13.2	14.1	13.9
Al_2O_3	11.61	11.97	12.06	11.91	11.39	Cs	4.07	3.89	3.78	3.83	3.63
Fe_2O_3	1.03	0.08	1.26	0.9	1.36	Ba	941	791	610	580	564
FeO	2.21	2.87	1.9	2.26	1.87	Hf	5.04	4.6	4.99	4.61	4.87
TiO_2	0.08	0.06	0.08	0.07	0.08	Ta	1.51	1.52	1.35	1.47	1.35
CaO	1.29	1.55	1.58	1.87	0.88	Pb	23.2	26.5	25.4	27.9	20.3
MgO	1.26	1.23	1.23	1.25	1.24	Th	27.6	27	24.8	26.9	24.4
K_2O	2.46	2.6	2.59	2.54	2.44	U	8.58	5.86	6.12	6.34	7.58
Na_2O	0.12	0.12	0.11	0.12	0.1	La	24.9	22.3	28.4	24.7	21.7
MnO	0.05	0.05	0.06	0.06	0.04	Ce	57.7	51.6	62.2	51.8	50.6
P_2O_5	0.01	0.01	0.01	0.01	0.01	Pr	6.63	5.8	7.08	6.47	5.89
LOI	3.37	3.66	3.74	3.89	3.03	Nd	26.1	22.5	27.9	24.3	22.1
Total	99.32	99.21	99.54	100.19	99.26	Sm	5.47	4.86	5.87	5.24	4.67
SiO_2/Al_2O_3	6.53	6.27	6.21	6.32	6.74	Eu	0.59	0.55	0.64	0.59	0.52
TiO_2/Al_2O_3	0.0069	0.005	0.0066	0.0059	0.007	Gd	5.17	4.86	5.87	5.24	4.67
A/CNK	1.3	1.73	1.24	1.45	1.24	Tb	0.98	0.91	1.09	0.99	0.85
Mg#	41.73	42.7	41.96	42.06	41.68	Dy	6.34	5.7	6.86	6.03	5.43
Li	29.1	23	24.8	24.3	25.6	Ho	1.22	1.09	1.34	1.16	1.03
Sc	4.66	4.28	4.63	3.79	4.13	Er	3.28	2.94	3.77	3.19	2.8
V	1.91	1.26	1.51	1.35	1.73	Tm	0.46	0.42	0.56	0.44	0.38
Cr	10.3	4.1	4.29	5.71	4.98	Yb	3.03	2.8	3.93	2.81	2.6
Co	1.71	1.27	1.32	1.3	1.36	Lu	0.46	0.42	0.61	0.43	0.4
Ni	4.02	1.38	1.89	2.2	1.86	ΣREE	142.33	126.75	156.28	133.4	123.57
Cu	2.23	1.55	1.75	1.65	1.87	δEu	0.33	0.34	0.33	0.34	0.34
Zn	43.4	36.8	35.9	38.7	38.4	LREE/HREE	5.8	5.62	5.46	5.57	5.83
Ga	15.8	13.8	14.6	14.1	13.8	$(La/Yb)_{CN}$	5.54	5.37	4.87	5.93	5.63
Rb	119	110	112	107	106	$(La/Sm)_{CN}$	2.86	2.89	3.04	2.97	2.92
Sr	85.7	73.6	68.6	73.3	58.9	$(Gd/Lu)_{CN}$	1.4	1.44	1.23	1.52	1.43
Y	33.9	29.3	39.3	32.1	29.8	Zr/Hf	23.41	21.67	23.64	22.12	24.22
Zr	118	99.7	118	102	118	Nb/Ta	10.26	9.21	9.77	9.59	10.29

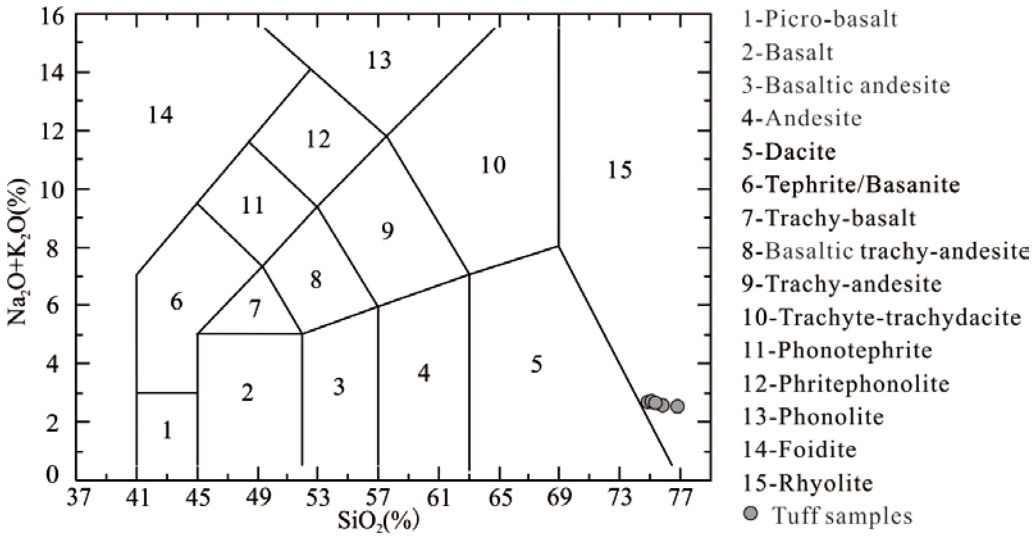

Figure 4. Total alkali–silica classification of the CTR

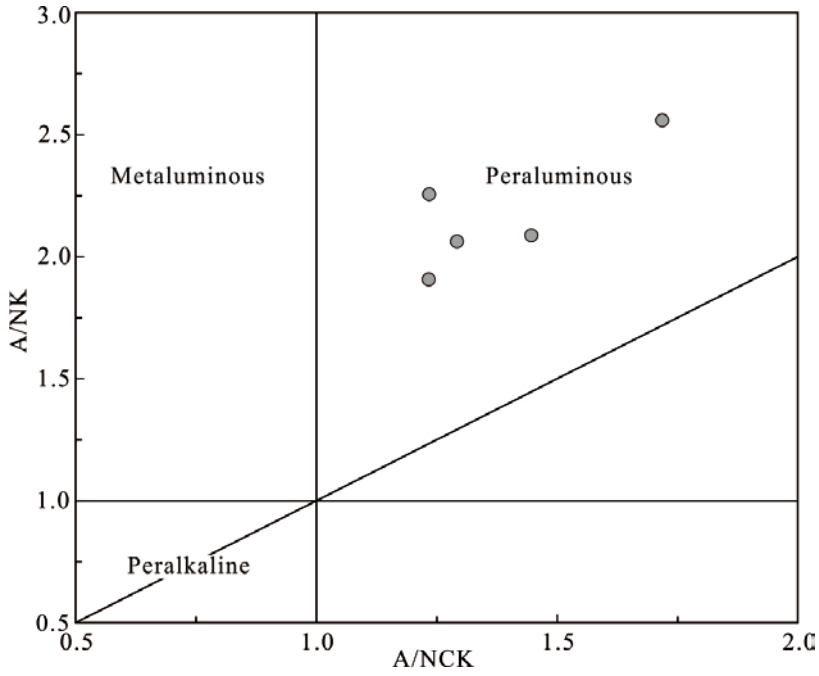

Figure 5. A/NK-A/CNK diagram of the CTR

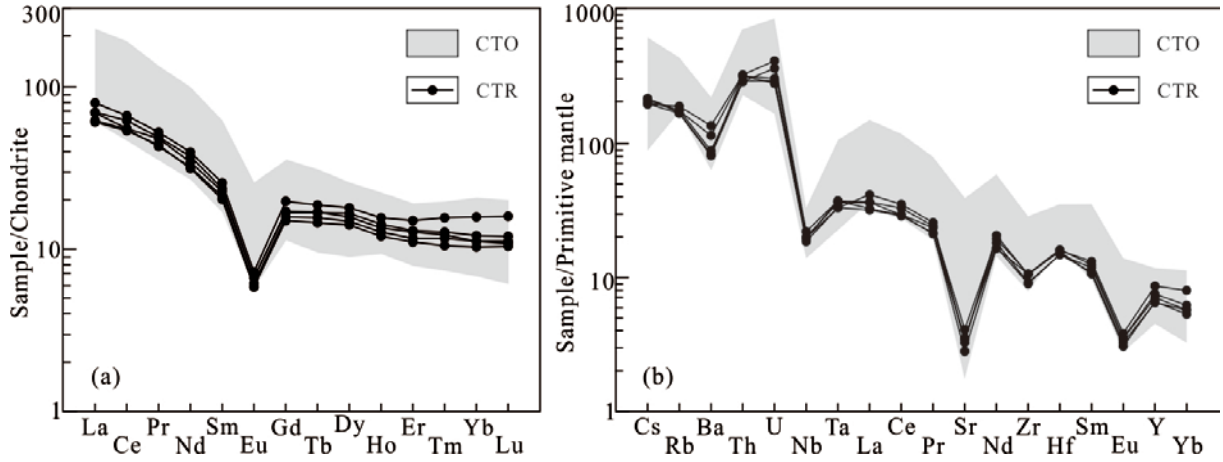

Figure 6. REE distribution pattern (a) and spidergram (b) of the CTR and CTO (The major and trace element data of the CTO are from Qiu et al., 2011, 2014).

4.2 Zircon analysis

Magmatic zircons generally display typical oscillation rings or sector zoning structures. The crystal form is often hypautomorphic or automorphic (Wu & Zheng, 2004). The CL images of zircons from the CTR show typical magmatic growth oscillation rings and rhythmic structures, suggesting a magmatic origin. The crystals are sound, crack-free, clean and transparent (Fig. 7). Studies have demonstrated different U and Th contents and Th/U ratios for zircons of different origins. Magmatic zircons have a higher Th and U content and a larger Th/U ratio (normally >0.4), whereas metamorphic zircons have a lower Th and U content and a smaller Th/U ratio (normally <0.1) (Rubatto & Gebauer, 1996; Hoskin & Schaltegger, 2003; Moller et al., 2003; Wu & Zheng, 2004). We selected euhedral zircons and measured 12 spots. The results show a Th content range of 175–716.5 ppm, a U content range of 241.8–1236.4 ppm, and a Th/U ratio range of 0.4–1.06. Obviously, the U and Th contents and the Th/U ratio of zircons from the CTR (Table 2) indicate the magmatic origin of the zircons. Also, taking into account the CL images of these zircons, we can conclude that all the zircons from the CTR are magmatogenic. The U-Pb zircon dating yielded a concordia age of 231.2 ± 1.4 Ma (Table 2, Fig. 8), which represents the age of volcanic eruptions.

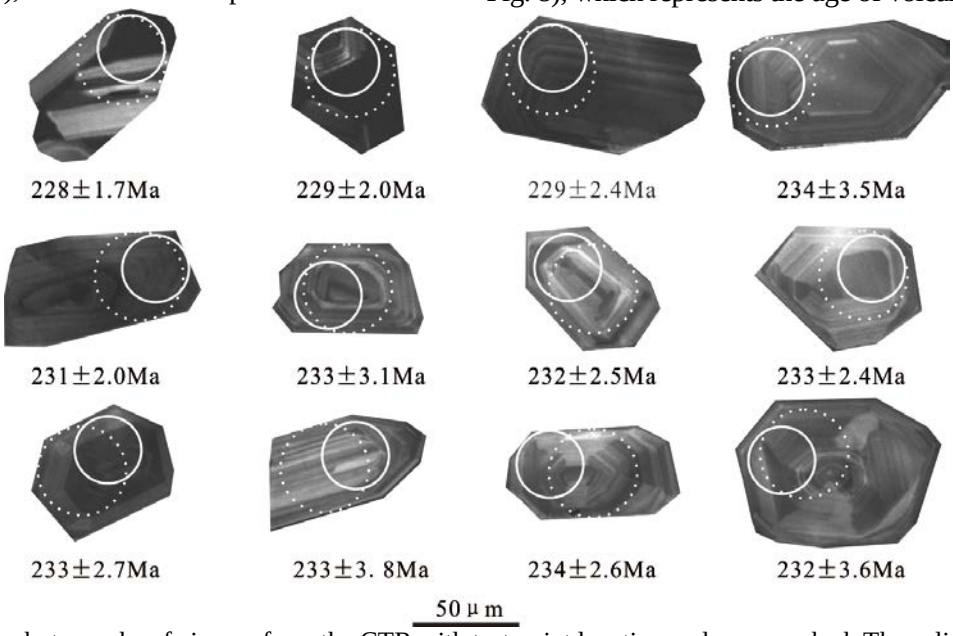

Figure 7. CL photographs of zircons from the CTR with test point location and ages marked. The solid line circles indicate the positions for U-Pb analysis and the dotted circles indicate the positions for Hf isotope analyses.

Table 2. Zircon dating data of CTR

Test point	Content ($\times10^{-6}$)			Th/U	Isotope ratio						Age (Ma)					
	Pb	Th	U		$\frac{^{207}Pb}{^{206}Pb}$	1	$\frac{^{207}Pb}{^{235}U}$	1	$\frac{^{207}Pb}{^{238}U}$	1	$\frac{^{207}Pb}{^{206}Pb}$	1	$\frac{^{207}Pb}{^{235}U}$	1	$\frac{^{207}Pb}{^{238}U}$	1
Ru.01	54.3	580.2	1236.4	0.47	0.0541	0.0009	0.2687	0.0046	0.0360	0.0003	376	37.0	242	3.7	228	1.7
Ru.02	34.0	716.5	678.5	1.06	0.0502	0.0012	0.2505	0.0060	0.0362	0.0003	211	55.6	227	4.9	229	2.0
Ru.03	18.4	221.2	432.7	0.51	0.0537	0.0014	0.2658	0.0063	0.0362	0.0004	367	57.4	239	5.1	229	2.4
Ru.04	42.8	400.6	990.9	0.40	0.0540	0.0016	0.2741	0.0064	0.0370	0.0006	372	66.7	246	5.1	234	3.5
Ru.05	46.9	505.4	1083.5	0.47	0.0519	0.0011	0.2605	0.0054	0.0365	0.0003	280	50.0	235	4.4	231	2.0
Ru.07	18.1	254.6	393.1	0.65	0.0557	0.0027	0.2825	0.0135	0.0369	0.0005	443	107.4	253	10.7	233	3.1
Ru.08	16.1	188.5	368.6	0.51	0.0559	0.0023	0.2818	0.0109	0.0366	0.0004	456	123.1	252	8.7	232	2.5
Ru.09	41.2	427.5	943.3	0.45	0.0503	0.0012	0.2573	0.0063	0.0369	0.0004	209	57.4	232	5.1	233	2.4
Ru.11	22.1	270.8	509.6	0.53	0.0512	0.0016	0.2586	0.0076	0.0368	0.0004	256	70.4	233	6.1	233	2.7
Ru.12	12.8	184.9	289.0	0.64	0.0498	0.0025	0.2501	0.0119	0.0368	0.0006	187	116.7	227	9.7	233	3.8
Ru.13	29.3	439.6	646.9	0.68	0.0539	0.0021	0.2737	0.0102	0.0369	0.0004	365	87.0	246	8.1	234	2.6
Ru.14	10.9	175.0	241.8	0.72	0.0511	0.0031	0.2587	0.0164	0.0367	0.0006	243	145.4	234	13.2	232	3.6

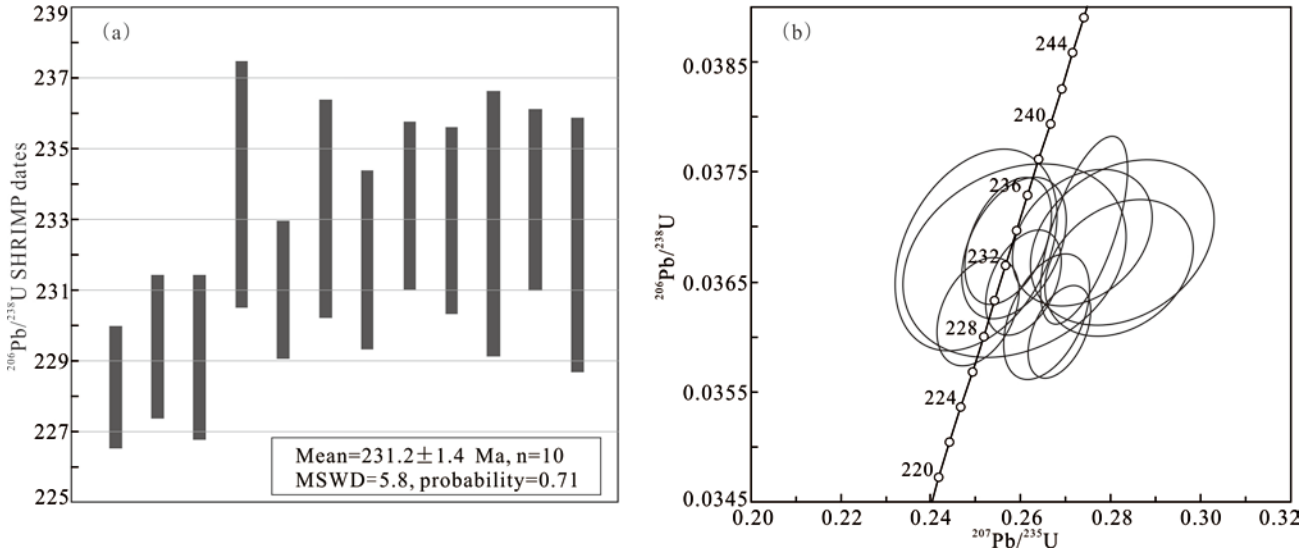

Figure 8. Weighted mean $^{206}Pb/^{238}U$ SHRIMP dates (a) and associated U-Pb concordia curve plots (b) for the CTR

4.3 Hf isotopic characteristics of zircons obtained from the CTR

Zircon has strong stability, so that its Hf isotope is less affected in the later geological time. The extremely low Lu content can be used to obtain the accurate Hf isotopic composition of zircon when it formed. These characteristics make Lu–Hf isotopes become an important tool to explore the evolution of the crust and trace the source of the rocks (Amelin et al., 1999).

For this study, we conducted analyses of the Lu–Hf isotopes in the zircons of CTR. The used analytical points coincided with or were in the same oscillatory zones as the U–Pb age dating points, ensuring that zircons of the same age were analyzed.

The results of Lu–Hf isotope analysis are shown in Table 3. The $^{176}Lu/^{177}Hf$ ratio of the CTR is less than 0.002, showing the zircon accumulated less radiogenic Hf after it formed. The measured $^{176}Lu/^{177}Hf$ ratio can better reflect the Hf isotopic composition of zircon in its formation process. The $^{176}Hf/^{177}Hf$ ratio of the analytical points ranges from 0.28253123 to 0.28262111, and the $\varepsilon_{Hf}(t)$ value ranges from -3.857 to -0.722 (with an average of -2. 17).

The $f_{Lu/Hf}$ ratio of zircons (averaging -0.97) are significantly less than the $f_{Lu/Hf}$ ratio of continental crust, thus the two-stage model age can correctly reflect the time when the source materials were extracted from the depleted mantle (Wu et al., 2007). The REE patterns suggest that the parent rocks of the CTR are granitic, therefore, the Lu/Hf ratio of the sialic crust was used in the calculation of the $t_{DM2}(Hf)$. The two-stage Hf-isotope model ages of the CTR range from 1297 to 1495 Ma (Table 3).

Table 3. Hf isotopic compositions for zircons obtained from the CTR

Test point	t (Ma)	1σ	$^{176}Lu/^{177}Hf$	2σ	$^{176}Hf/^{177}Hf$	2σ	$\varepsilon_{Hf}(0)$	$\varepsilon_{Hf}(t)$	2σ	T_{DM1}	T_{DM2}	$f_{Lu/Hf}$
Ru.01	228	4	0.001413934	2.32253E-06	0.28261707	1.926E-05	-5.479	-0.83	0.702	908.83	1303	-0.957
Ru.02	229	4	0.001773408	1.96269E-05	0.28259791	1.678E-05	-6.1564	-1.56	0.617	945.21	1350	-0.947
Ru.03	229	4	0.002177969	3.8177E-05	0.28260142	3.049E-05	-6.0322	-1.495	1.091	950.57	1346	-0.934
Ru.04	234	4	0.0027597	2.86007E-05	0.28261042	2.506E-05	-5.714	-1.262	0.901	952.66	1331	-0.917
Ru.05	231	4	0.00165526	1.56491E-05	0.28262111	2.266E-05	-5.3362	-0.722	0.819	908.97	1297	-0.95
Ru.07	233	4	0.001002606	2.72453E-06	0.28253371	2.233E-05	-8.4271	-3.719	0.808	1016.2	1486	-0.97
Ru.08	232	4	0.001350313	2.15562E-05	0.28253123	2.693E-05	-8.5146	-3.857	0.968	1029.2	1495	-0.959
Ru.09	233	4	0.002334376	1.23074E-05	0.28254581	2.855E-05	-7.9991	-3.486	1.023	1035.7	1471	-0.93
Ru.11	233	4	0.001478325	3.82881E-05	0.28256337	2.192E-05	-7.3779	-2.739	0.794	986.93	1424	-0.955
Ru.12	233	4	0.00159611	9.61048E-06	0.28256001	2.325E-05	-7.4967	-2.875	0.84	994.86	1433	-0.952
Ru.13	234	4	0.001450941	9.10601E-06	0.28258636	1.864E-05	-6.5651	-1.922	0.681	953.49	1373	-0.956
Ru.14	232	4	0.001341344	1.28092E-05	0.28259458	2.056E-05	-6.2744	-1.615	0.747	939.02	1353	-0.96

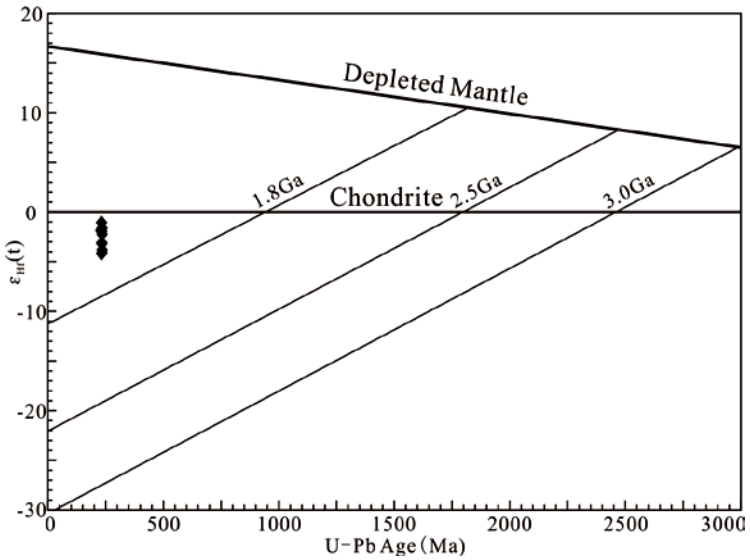

Figure 9. ε_{Hf} (t) vs U-Pb age diagram for zircons obtained from the CTR

5. DISCUSSION

5.1 The affinity between the CTR and CTO

In order to determine the relationship between the CTR and CTO, this paper comparatively analyzed their zircon U-Pb ages, geochemical characteristics and Hf isotope characterization. The REE distribution pattern and spidergram of the CTR present a consistency with the CTO (Fig. 6): (1) REE distribution patterns of the CTR and CTO show a negative Eu anomaly, and the chondrite-normalized REE diagram displays a rightward inclined slope of LREE with flat HREE trend. (2) Both CTR and CTO show strong positive anomalies of Rb, Th and U, and negative anomalies of Nb, Sr and Eu on a primitive mantle-normalized spidergram. LA-ICP-MS zircon U-Pb data shows that the crystallization age of the CTR is 231.2 ± 1.4 Ma, which is consistent with the zircon U–Pb age of 205～242 Ma for the CTO (Deng et al., 2008, 2009; Zhang et al., 2009a, 2014; Yang & Deng, 2013; Wang et al., 2014). Their Hf isotope characterizations are also extremely similar: (1) The $\varepsilon_{Hf}(t)$ value of the CTR ranges from -3.857 to -0.722 (with an average of -2.17), and that of the CTO ranges from -6.6 to 1.6 (with an average of -2.4) (Zhang et al., 2014), (2) The two-stage Hf-isotope model ages of the CTR range from 1.3 Ga to 1.5 Ga, and that of the CTO ranges from 1.1 Ga to 1.3 Ga (Zhang et al., 2014). Their Hf isotope characterization indicates that all the Chang 7 tuffs sampled from these two places mainly originated from partial melting of the Mesoproterozoic to Neoproterozoic crustal material.

In summary, because of the similar zircon U-Pb ages, geochemical characteristics and Hf isotope characterization, the CTR and CTO were products of volcanic activity in the same tectonic setting. Because the former covers a wider range, it should correspond to the most intense volcanic eruption in the Qinling orogenic belt.

5.2 Magmatic origin

In the SiO_2 — K_2O + Na_2O diagram, all samples are plotted in the rhyolite area. This shows that the CTR is rhyolitic tuff. The experimental petrology study shows that the rhyolitic magma originated from the partial melting of the mid-crustal rocks, and it cannot originate from the partial melting of peridotite in the upper mantle (Rushmer, 1991; Beard & Lofgren, 1991; Hirose, 1997). The element geochemistry theory suggests that the geochemical behavior of Sr, Ba, Eu and Ca are similar, and the geochemical behavior of Sr and Ba in the endogenous processes depends on the original concentration of Ca in magmatic melts (Liu et al, 1984; Wang et al., 1989; Li 1992; Lai et al., 2006). The rhyolitic tuff shows strong negative anomalies in Sr and Ba. This suggests that the rhyolite originated from the lower crust, where the plagioclase is stable (Defant & Drummond, 1993), or it experienced a more significant fractionation of plagioclase during the ascent of the primary magma.

Distinctly from the steep HREE distribution pattern of the modern adakites (Drummond et al., 1996; Martin, 1999), the CTR shows a relatively flat HREE distribution pattern. This suggests that the residue of partial melting contains amphibole, but not garnet. The low TiO_2 content of CTR may be related to this. According to the results of experimental petrology, at the pressure-temperature conditions of 850-1100°C and <1.0 GPa, the hornblende and plagioclase coexist as residual phases of partial

melting without reacting to form garnet (Lai et al., 2006). This, in conjunction with the formation of rhyolitic magma at pressure greater than 0.5 GPa, suggests that the parental magma originated from the lower, crust at depths from 35 to 15 km.

The $\varepsilon_{Hf}(t)$ value of CTR ranges from -3.857 to -0.722, with an average of -2.17. In the T-$\varepsilon_{Hf}(t)$ diagram, all points are plotted under the chondrite, showing that the tuffs originated from the partial melting of ancient crust. The two-stages Hf-isotope model ages of the CTR range from 1297 to 1495 Ma, which is significantly greater than its formation age (228 to 234 Ma). This indicates that the CTR mainly originated from Mesoproterozoic crustal material (Fig. 9).

Considering the lack of evidence of volcanic eruptions in the Ordos Basin during the deposition of the CTO and CTR, the vents were most likely located outside the basin. Previous research suggests a clear decrease in the total thickness of Chang7 tuff intervals toward the northeastern Ordos Basin (Fig.1), indicating that these tuffs are from the southwestern part of the Ordos basin or south of this basin (Deng et al., 2008, 2009; Qiu et al., 2011, 2014).

Zhang et al., (2014) thought the parental magma of the Chang7 tuff intervals in the southwestern part of Ordos Basin are a mixture of Yaolinghe Group basic volcanic rocks and Yunxi Group acid volcanic rocks from the basement of the South Qinling Orogenic belt. However, considering that the Yaolinghe Group mainly consists of basic volcanic rocks metamorphosed under greenschist or amphibolite facies conditions, these could not be partially melted to produce granitic magma (Zhang et al., 2002). Therefore, these basic volcanic rocks are not the source rocks of Chang7 rhyolitic tuffs.

The two-stage Hf-isotope model ages of CTR is older than that produced by the Indosinian granites from the south Qinling Orogenic belt (1.3-0.9 Ga) (Gong et al., 2009; Qin et al., 2010, 2013), but similar to that of the Indosinian granites from the eastern part of the west Qinling Orogenic belt (1.5-1.3 Ga) (Li et al., 2015; Luo et al., 2015; Huang, 2016; Ren et al., 2016; Wang et al., 2016). Based on the T_{DMC} comparison, the Chang7 tuffs and the Indosinian granites from the eastern part of west Qinling Orogenic belt have the same parental magma. Ancient basement is hardly found in the west Qinling Orogenic belt, while the Nd model ages of Indosinian granites yield two peaks at ~1.51 Ga and ~1.35 Ga (Zhang et al., 2002; Huang, 2016). That means the lower crust of west Qinling Orogenic belt is mainly composed of two stages Mesoproterozoic extracts from mantle, which correlate well with the Mesoproterozoic crustal accretion on the northwestern margin of Yangtze block (Zhang et al., 2002). It can be concluded that the Mesoproterozoic crust which similar to that in Yangtze block is existing in the west Qinling Orogenic belt. The Chang7 tuffs and the granites in the eastern part of west Qinling Orogenic belt might come from the partial melting of Mesoproterozoic metamorphic basement of the west Qinling Orogenic belt.

5.3 Tectonomagmatic setting

In order to determine the possible tectonic setting of the volcanoes responsible for the CTR, we plotted the tuff data on the bivariate plots of Nb versus Y (Fig. 10a) and Rb versus Y + Nb (Fig. 10b), which are used for discriminating the tectonic setting of granitic rocks (Pearce et al., 1984). Most of the CTR data fall in the ‘‘volcanic-arc granite’’ field, suggesting the derivation of the CTR from an arc-related source.

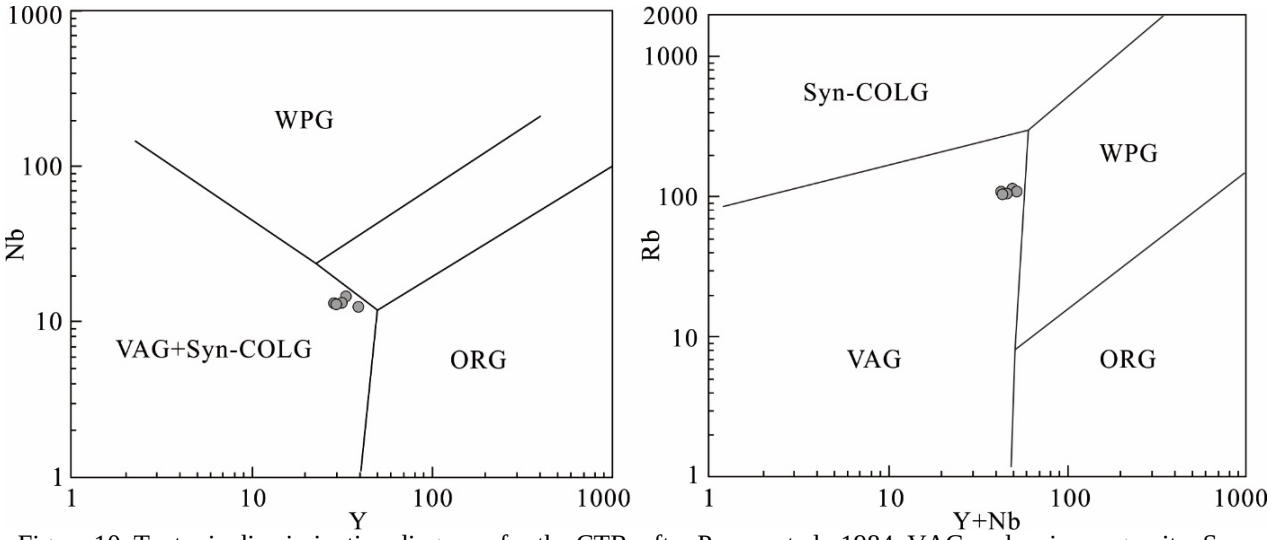

Figure 10. Tectonic discrimination diagrams for the CTR, after Pearce et al., 1984. VAG: volcanic arc granite; Syn-COLG: syn-collisional granite; WPG: within plate granite; ORG: ocean ridge granite.

According to previous research, it is widely accepted that the A'nyemaqen–Mianlue Ocean was subducted northward in Late Paleozoic and then it closed in the Middle-Late Triassic (Zhang et al., 2001, 2004; Meng et al., 2005; Jiang et al., 2010; Dong et al., 2012; Ni et al., 2012; Li et al., 2013, 2014; Qiu et al., 2014). The closure of A'nyemaqen–Mianlue Ocean caused the collision of the South China blocks with the South Qinling orogen along the Mianlue suture belt that led to final integration of the North and South China blocks. Many metavolcanic rocks of 220 ～245 Ma were well dated along this suture belt showing the collision time (Li et al., 1996, 2015; Lai et al., 1998; Gong et al., 2009; Cao et al., 2011; Zhang et al., 2009b; Liu et al., 2011). The depositional age of the CTR ranges from 228 to 234 Ma, which is consistent with the subduction time of A'nyemaqen–Mianlue Ocean and collision time of North China block and Yangtze block. Therefore, the formation of CTR may relate to the volcanic arc formed during the subduction of the A'nyemaqen–Mianlue Ocean.

6. CONCLUSION

1. The U-Pb dating result of the CTR are within the age interval of 242～205 Ma for CTO, and the CTR have similar geochemical and Hf isotopic characteristics with CTO, thus they are the product of volcanic eruption in the same tectonic setting. Due to the wider coverage, the CTR should correspond to the most intense volcanic eruption in the Qinling orogenic belt.

2. The geochemical composition of CTR shows that the magma originated from the partial melting of the lower crust, whose depth ranges from 35 to 15 km. The two-stage Hf-isotope model ages of the CTR ranges from 1297 to 1495 Ma, indicating that they mainly derive from Mesoproterozoic crustal material.

3. Major and trace element data suggests that the tectonomagmatic origin of the CTR was related to a volcanic arc. LA-ICP-MS zircon U-Pb data shows that CTR crystallized at 231.2 ± 1.4 Ma, which is consistent with the subduction time of A'nyemaqen–Mianlue Ocean, thus the formation of the CTR may be related to volcanic arc in the process of subduction.

REFERENCES

Amelin, Y., Lee D.C., Halliday A. N., & Pidgeon R. T., 1999. *Nature of the Earth's earliest crust from hafnium isotopes in single detrital zircons.* Nature, 399, 252-255.

Andersen, T., 2002. *Correction of common lead in U–Pb analyses that do not report ^{204}Pb.* Chemical geology, 192, 1, 59-79.

Beard J.S., & Lofgren G.E., 1991. *Dehydration melting and water-saturated melting of basaltic and andesitic greenstones and amphibolites at 1, 3, and 6. 9 kb.* Journal of Petrology, 32, 2, 465-501.

Blichert-Toft, J., & Albarède, F., 1997. *The Lu-Hf isotope geochemistry of chondrites and the evolution of the mantle-crust system.* Earth and Planetary Science Letters, 148, 1, 243-258.

Burger, K., Zhou, Y.P., & Ren, Y.L., 2002. *Petrography and geochemistry of tonsteins from the 4th member of the Upper Triassic Xujiahe formation in southern Sichuan province, China.* International Journal of Coal Geology, 49, 1-17.

Cao, X.F., Lu, X.B., Yao, S.Z., Mei, W., Zou, X.Y., Chen, C., Liu, S.T., Zhang, P., Su, Y.Y., & Zhang, B., 2011. *LA–ICP-MS U–Pb zircon geochronology, geochemistry and kinetics of the Wenquan ore-bearing granites from West Qinling, China.* Ore Geology Reviews, 43, 120-131.

Chu, N.C., Taylor, R.N., Chavagnac, V. Nesbitt, R.W., Boella, R.M., Milton, J.A., German, C.R., Bayon, G., & Burton, K., 2002. *Hf isotope ratio analysis using multi-collector inductively coupled plasma mass spectrometry: an evaluation of isobaric interference corrections.* Journal of Analytical Atomic Spectrometry, 17, 12, 1567-1574.

Defant, M.J., & Drummond, M.S., 1993. *Mount St. Helens: Potential example of the partial melting of the subducted lithosphere in a volcanic arc.* Geology, 21, 6, 547-550.

Deng, X.Q., Li, W.H., Liu, X.S., Pang, J.L., & Liu, X., 2009. *Discussion on the stratigraphic boundary between Middle Triassic and Upper Triassic.* Acta Geologica Sinica, 83, 8, 1089-1096 (in Chinese with English abstract).

Deng, X.Q., Liu, F.X., Liu, X.Y., Pang, J.L., Lv, J.W., Li, S.X., & Liu, X., 2008. *Discussion on relationship between sedimentary evolution of the Triassic Yanchang Formation and the Early Indosinian movement in Ordos Basin.* Journal of Palaeogeography, 10, 2, 159-166 (in Chinese with English abstract).

Deng, X.Q., Luo, A.X., Zhang, Z.Y., & Liu, X., 2013. *Geochronological Comparison on Indosinian Tectonic Events between Qinling Orogeny and Ordos Basin.* Acta Sedimentologica Sinica, 31, 6, 939-953 (in Chinese with English abstract).

Dong, Y.P., Liu, X.M., Zhang, G.W., Chen, Q., Zhang, X.N., Li, W. & Yang, C., 2012. *Triassic diorites and granitoids in the Foping area: Constraints on the conversion from subduction to collision in the Qinling orogeny, China.* Journal of Asian Earth Sciences, 47, 1, 123-142.

Drummond, M.S., Defant, M.J., & Kepezhinskas, P.K., 1996. *Petrogenesis of slab-derived trondhjemite-tonalite-dacite/adakite magmas.* Earth & Environmental Science Transactions of the Royal Society of Edinburgh, 87, 1-2, 205-215.

Eggins, S.M., Kinsley, L.P.J., & Shelley, J.M.G., 1998. *Deposition and element fractionation processes during atmospheric pressure laser sampling for analysis by*

ICP-MS. Applied Surface Science, 127-129, 278-286.

Elhlou, S., Belousova, E., Griffin, W.L., Pearson, N.J., & O'Reilly, S.Y., 2006. *Trace element and isotopic composition of GJ-red zircon standard by laser ablation.* Geochimica et Cosmochimica Acta, 70, 18, A158.

Gong, H.J., Zhu, L.M., Sun, B.Y., Li, B., & Guo, B., 2009. *Zircon U-Pb ages and Hf isotope characteristics and their geological significance of the Shahewan, Caoping and Zhashui granitic plutons in the South Qinling orogen.* Acta Petrologica Sinica, 25, 2, 248-264 (in Chinese with English abstract).

Griffin, W.L., Wang, X., Jackson, S.E., Pearson, N.J., O'Reilly, S.Y., Xu, X., & Zhou, X., 2002. *Zircon chemistry and magma mixing, SE China: in-situ analysis of Hf isotopes, Tonglu and Pingtan igneous complexes.* Lithos, 61, 3, 237-269.

Haskin, L.A., Haskin, M.A., & Frey, F.A., 1968. *Relative and absolute terrestrial abundances of the rare earth. In: Ahrens, L.H. (Ed.), Origin and Distribution of the Elements.* Pergamon, Oxford, 1, 889-911.

Hirose, K., 1997. *Melting experiments on lherzolite KLB-1 under hydrous conditions and generation of high-magnesian andesitic melts.* Geology, 25, 1, 42-44.

Hoskin, P.W.O., & Schaltegger, U., 2003. *The composition of zircon and igneous and metamorphic petrogenesis.* Reviews in Mineralogy and Geochemistry, 53, 1, 27-62.

Hu, Z.C., Gao, S., Liu, Y.S., Hu, S.H., Chen, H.H., & Yuan, H.L., 2008. *Signal enhancement in laser ablation ICP-MS by addition of nitrogen in the central channel gas.* Journal of Analytical Atomic Spectrometry, 23, 8, 1093-1101.

Hu, Z.C., Liu, Y.S., Gao, S., Liu, W.Q., Zhang, W., Tong, X.R., Lin, L., Zong, K.Q., Li, M., Chen, H.H., Zhou, L. & Yang, L., 2012. *Improved in situ Hf isotope ratio analysis of zircon using newly designed X skimmer cone and jet sample cone in combination with the addition of nitrogen by laser ablation multiple collector ICP-MS.* Journal of Analytical Atomic Spectrometry, 27, 9, 1391-1399.

Huang, X.F., 2016. *Petrogenesis of the Indosinian granitic magmatism and tectonic evolution of the West Qinling Orogenic Belt.* A Dissertation Submitted to China University of Geosciences for Doctoral Degree (in Chinese with English abstract).

Huang, X.F., Shi, W., Chen, P., & Li, H.Q., 2015. *Superposed deformation in the Helanshan Structural Belt: Implications for Mesozoic intracontinental deformation of the North China Plate.* Journal of Asian Earth Sciences, 114, 10, 140-154.

Jackson, S.E., Pearson, N.J., Griffin, W.L., & Belousova, E.A., 2004. *The application of laser ablation-inductively coupled plasma-mass spectrometry to in situ U–Pb zircon geochronology.* Chemical Geology, 211, 1-2, 47-69.

Jiang, Y.H., Jin, G.D., Liao, S.Y., Zhou, Q. & Zhao, P., 2010. *Geochemical and Sr-Nd-Hf isotopic constraints on the origin of Late Triassic granitoids from the Qinling orogeny, central China: Implications for a continental arc to continent-continent collision.* Lithos, 117, 1-4, 183-197.

Lai, S.C., Zhang, G.W., Qin, J.F., Li, Y.F. & Liu, X., 2006. *Geochemistry and petrogenesis of the Tertiary rhyolite from the Boyang area, northeastern margin of the Qinghai-Tibet plateau.* Earth Science Frontiers, 13, 4, 212-220 (in Chinese with English abstract).

Lai, S.C., Zhang, G.W., Yang, Y.C., & Chen, J.Y., 1998. *Geochemistry of the ophiolite and island arc volcanic rock in the Mianxian-Lueyang suture zone, Southern Qinling and their tectonic significance.* Chinese Journal of Geochemistry, 18, 1, 39-50 (in Chinese with English abstract).

Li N., Chen Y. J., Santosh M., & Pirajno, F., 2015. *Compositional polarity of Triassic granitoids in the Qinling Orogen, China: Implication for termination of the northernmost paleo-Tethys.* Gondwana Research, 27, 1, 244-257.

Li, C.N. 1992. *Trace Element Petrology of igneous Rocks.* China University of Geosciences Press, Wuhan (in Chinese).

Li, L., Meng, Q.R., Pullen, A., Garzione, C.N., Wu, G.L., Wang, Y.L., Ma, S.X., & Duan, L., 2014. *Late Permian-early Middle Triassic back-arc basin development in West Qinling, China.* Journal of Asian Earth Sciences, 87, 12, 116-129.

Li, S.G., Sun, W.D., Zhang, G.W., Chen, J.Y., & Yang, Y.C., 1996. *Chronology and geochemistry of metavolcanic rocks from Heigouxia Valley in the Mianlve tectonic zone, South Qinling: Evidence for a Paleozoic oceanic basin and its close time.* Science in China (Series D), 39, 300-310.

Li, X.W., Mo, X.X., Huang, X.F., Dong, G.C., Yu, X.H., Luo, M.F., & Liu, Y.B., 2015. *U-Pb zircon geochronology, geochemical and Sr-Nd-Hf isotopic compositions of the Early Indosinian Tongren Pluton in West Qinling: Petrogenesis and geodynamic implications.* Journal of Asian Earth Sciences, 97, 38-50.

Li, X.W., Mo, X.X., Yu, X.H., Ding, Y., Huang, X.F., Wei, P., & He, W.Y., 2013. *Petrology and geochemistry of the Early Mesozoic pyroxene andesites in the Maixiu area, West Qinling, China: Products of subduction or syn-collison?* Lithos, 172-173, 158-174.

Liu, C.Y., Qiu, X.W., Wu, B.L., & Zhao, H.G., 2007. *Characteristics and dynamic settings of Central-east Asia muti-energy minerals metallogenetic domain.* Science in China (Series D), 50, Supp. II, 1-18.

Liu, C.Y., Zhao, H.G., Gui, X.j., Yue, L.P., Zhao, J.F., & Wang, J.Q., 2006. *Space-Time Coordinate of the Evolution and Reformation and Mineralization Response in Ordos Basin.* Acta Geologica Sinica, 80, 5, 617-638 (in Chinese with English abstract).

Liu, C.Y., Zhao, H.G., Wang, F., Feng, & Chen, H., 2005. *Attributes of the Mesozoic Structure on the West Margin of the Ordos Basin.* Acta Geologica Sinica, 79, 6, 737-747(in Chinese with English abstract).

Liu, S.F., 1998. *The coupling mechanism of Basin and Orogen in the western Ordos Basin and adjacent regions of China.* Journal of Asian Earth Sciences, 16,

4, 369-383.

Liu, S.F., Su, S., & Zhang, G.W., 2013. *Early Mesozoic basin development in North China: Indications of cratonic deformation.* Journal of Asian Earth Sciences, 62, 221-236.

Liu, Y.J., Cao, L.M., Li, Z.L., Wang, H.N., Chu, T.Q., & Zhang, J.R., 1984. *Element Geochemistry.* Science Press, Beijing (in Chinese).

Liu, Y.S., Gao, S., Hu, Z.C., Gao, C.G., Zong, K.Q., & Wang, D.B., 2010a. *Continental and oceanic crust recycling-induced melt-peridotite interactions in the Trans-North China Orogen: U–Pb dating, Hf isotopes and trace elements in zircons from mantle xenoliths.* Journal of Petrology, 51, 537-571.

Liu, Y.S., Hu, Z.C., Gao, S., Günther, D., Xu, J., Gao, C.G., & Chen, H.H., 2008. *In situ analysis of major and trace elements of anhydrous minerals by LA-ICP-MS without applying an internal standard.* Chemical Geology, 257, 1, 34-43.

Liu, Y.S., Hu, Z.C., Zong, K.Q., Gao, C.G., Gao, S., Xu, J., & Chen, H.H., 2010b. *Reappraisement and refinement of zircon U–Pb isotope and trace element analyses by LA–ICP–MS.* Chinese Science Bulletin, 55, 15, 1535-1546.

Ludwig, K.R., 2012. *User's Manual for Isoplot 3.75: A Geochronological Toolkit for Microsoft Excel.* Berkeley Geochronology Center Special Publication No. 5, 1-75.

Luo, B.J., Zhang, H.F., Xu, W.C., Guo, L., Pan, F.B., & Yang, H., 2015. *The Middle Triassic Meiwu batholith, West Qinling, Central China: Implications for the evolution of compositional diversity in a composite batholith.* Journal of Petrology, 56, 6, 1139-1172.

Martin, H., 1999. *Adakitic magmas: Modern analogues of Archean granitoids.* Lithos, 46, 3, 411-429.

McLennan, S.M., 1989. *Rare earth elements in sedimentary rocks: influence of provenance and sedimentary processes.* Reviews in Mineralogy and Geochemistry, 21, 169-200.

Meng, Q.R., Wang, E., & Hu, J.M., 2005. *Mesozoic sedimentary evolution of the Northwest Sichuan basin: Implication for continued clockwise rotation of the South China block.* Geological Society of America Bulletin, 117, 3, 396-410.

Moller, A., O'Brien, P.J., Kennedy, A. & Kroner, A., 2003. *Linking growth episodes of zircon and metamorphic textures to zircon chemistry: An example from the ultrahigh-temperature granulites of Rogaland (SW Norway).* Geological Society, London, Special Publications, 220, 1, 65-82.

Münker, C., 1998. *Nb/Ta fractionation in a Cambrian arc/back arc system, New Zealand: source constraints and application of refined ICPMS techniques.* Chemical Geology, 144, 1-2, 23-45.

Ni, Z.Y., Chen, Y.J., Li, N. & Zhang, H., 2012. *Pb-Sr-Nd isotope constraints on the fluid source of the Dahu Au-Mo deposit in Qinling Orogen, central China, and implication for Triassic tectonic setting.* Ore Geology Reviews, 46, 8, 60-67.

Pearce, J.A., Harris, N., & Tindle, A., 1984. *Trace element discrimination diagrams for the tectonic interpretation of granite rocks.* Journal of Petrology, 15, 956-983.

Qin, J.F., Lai, S.C., Diwu, C.R., Ju, Y.J. & Li, Y.F., 2010. *Magma mixing origin for the postcollisional adakitic monzogranite of the Triassic Yangba pluton, Northwestern margin of the South China block: geochemistry, Sr–Nd isotopic, zircon U–Pb dating and Hf isotopic evidences.* Contributions to Mineralogy and Petrology, 159, 3, 389–409.

Qin, J.F., Lai, S.C. & Li, Y.F., 2013. *Multi-stage granitic magmatism during exhumation of subducted continental lithosphere: Evidence from the Wulong pluton, South Qinling.* Gondwana Research, 24, 3-4, 1108-1126.

Qiu, X.W., Liu, C.Y., Li, Y.H., Mao, G.Z., & Wang, J.Q., 2009. *Distribution characteristics and geological significances of tuff interlayers in Yanchang formation of Ordos Basin, China.* Acta Sedimentologica Sinica, 27, 5, 1138-1146 (in Chinese with English abstract).

Qiu, X.W., Liu, C.Y., Mao, G.Z., Deng, Y. & Wang, F.F., 2010. *Enrichment feature of thorium element in tuff interlayers of Upper Triassic Yanchang formation in Ordos Basin, China.* Geological Bulletin of China, 29, 8, 1185-1191 (in Chinese with English abstract).

Qiu, X.W., Liu, C.Y., Mao, G.Z., & Wu, B.L., 2011. *Petrological-geochemical characteristics of volcanic ash sediments in Yanchang formation in Ordos Basin.* Earth Science–Journal of China University of Geosciences, 36, 1, 139-150 (in Chinese with English abstract).

Qiu, X.W., Liu, C.Y., Mao, G.Z., Deng, Y., Wang, F.F., & Wang, J.Q., 2014. *Late Triassic tuff intervals in the Ordos Basin, Central China: Their depositional, petrographic, geochemical characteristics and regional implications.* Journal of Asian Earth Sciences, 80, 148-160.

Qiu, X.W., Liu, C.Y., Wang, J.Q., Deng, Y., Wang, F.F., & Mao, G.Z., 2013. *Triggers and characteristics of late Triassic deep-lacustrine synsedimentary deformation structures in Ordos basin.* Chinese Journal of Geology, 48, 1, 204-216 (in Chinese with English abstract).

Ren, H.D., Wang, T., Zhang, L., Wang, X.X., Huang, H., Feng, C.Y., Teschner, C., & Song, P., 2016. *Ages, sources and tectonic settings of the Triassic igneous rocks in the easternmost segment of the East Kunlun Orogen, Central China.* Acta Geologica Sinica, 90, 2, 641-668.

Ritts, B.D., Hanson, A.D., Darby, B.J., Nanson, L., & Berry, A.K., 2004. *Triassic intraplate extension in North China: evidence from the nonmarine NW Ordos Basin.* Tectonophysics, 386, 177-202.

Rubatto, D., & Gebauer, D., 1996. *Use of cathodoluminescence for U-Pb zircon dating by ion microprobe (SHRIMP): Some examples from highpressure rocks of the Western Alps.* International Conference on Cathodoluminescence and Related Techniques in Geosciences and Geomaterials, 131-132.

Rushmer, T., 1991. *Partial melting of two amphibolites: contrasting experimental results under fluid-absent*

conditions. Contributions to Mineralogy and Petrology, 107, 1, 41-59.

Sun, S.S., & McDonough, W.F., 1989. *Chemical and isotopic systematics of oceanic basalts: implications for mantle composition and process from. In: Saunders, A.D., Norry, M.J. (Eds.), Magmatism in the Ocean Basins.* Geological Society Special Publication, 42, 313-345.

Wang, D.Y., Xin, B.S., Yang, H., Fu, J.H., Yao, J.L. & Zhang, Y., 2014. *Zircon SHRIMP U-Pb age and geological implications of tuff at the bottom of Chang-7 Member of Yanchang Formation in the Ordos Basin.* Science in China (Series D), 57, 2, 2160-2171.

Wang, H., Feng, C.Y., Li, D.X., Li, C., Ding, T.Z., & Liao, F.Z., 2016. *Geology, geochronology and geochemistry of the Saishitang Cu deposit, East Kunlun Mountains, NW China: Constraints on ore genesis and tectonic setting.* Ore Geology Reviews, 72, 43-59.

Wang, Z.G., Yu, X.Y., & Zhao, Z.H., 1989. *Geochemistry of rare earth elements.* Science Press, Beijing (in Chinese).

Woodhead, J.D., & Hergt, J. M., 2010. *A preliminary appraisal of seven natural zircon reference materials for in situ Hf isotope determination.* Geostandards and Geoanalytical Research, 29, 2, 183-195.

Wu, F.Y., Li, X.H., Zheng, Y.F., & Gao, S., 2007. *Lu-Hf isotopic systematics and their applications in petrology.* Acta Petrologica Sinica, 23, 2, 185-220.

Wu, F.Y., Yang, Y.H., Xie, L.W., Yang, J.H., & Xu, P., 2006. *Hf isotopic compositions of the standard zircons and baddeleyites used in U-Pb geochronology.* Chemical Geology, 234, 1-2, 105-126.

Wu, Y.B., & Zheng, Y.F., 2004. *Genesis of zircon and its constraints on interpretation of U-Pb age.* Chinese Science Bulletin, 49, 15, 1554-1569.

Yang, H., & Deng, X.Q., 2013. *Deposition of Yanchang formation deep-water sandstone under the control of tectonic events, Ordos basin.* Petroleum Exploration and Development, 40, 5, 513-520 (in Chinese with English abstract).

Zhang, B.R., Gao, S., Zhang, H.F., & Han, Y.W., 2002. *Geochemistry of Qinling Orogenic belt.* Science Press, Beijing, 1-187 (in Chinese).

Zhang, G.W., Dong, Y.P., Lai, S.C., Guo, A.L., Meng, Q.R., Liu, S.F., Cheng, S.Y., Yao, A.P., Zhang, Z.Q., & Pei, X.Z., 2004. *Mianlue tectonic zone and Mianlue suture zone on southern margin of Qinling-Dabie orogenic belt.* Science in China (Series D), 47, 4, 300-316.

Zhang, G.W., Zhang, B.R., Yuan, X.C. & Xiao, Q.H., 2001. *Qinling Orogenic Belt and Continental Dynamics.* Science Press, Beijing, 1-806 (in Chinese).

Zhang, H., Peng, P.A., & Zhang, W.Z., 2014. *Zircon U-Pb ages and Hf isotope Characterization and their Geological significance of Chang7 tuff of Yanchang Formation in Ordos Basin.* Acta Petrologica Sinica, 20, 2, 565-575 (in Chinese with English abstract).

Zhang, W.Z., Yang, H., Peng, P.A., Yang, Y.H., Zhang, H., & Shi, X.H., 2009a. *The Influence of Late Triassic volcanism on the development of Chang 7 high grade hydrocarbon source rock in Ordos Basin.* Geochimica, 38, 6, 573-582 (in Chinese with English abstract).

Zhang, C.L., Wang, X.X., Wang, T., & Dai, M.N., 2009b. *Origin of Shahewan granite intrusion in Eastern Qinling: evidence from zircon U–Pb dating and Hf isotopes.* Journal of Northwest Univerisity (Natural Science Eidtion), 39, 3, 453-465 (in Chinese with English abstract).

Zhao, H.G., Liu, C.Y., Wang, J.Q., Wang, F., & Yin, Y., 2007. *Tectonic attribute of the western Ordos Basin during the Late Triassic.* Geology in China, 34, 3, 384-391 (in Chinese with English abstract).

Zhou, Y.P., Bohor, B.F., & Ren, Y.L., 2000. *Trace element geochemistry of altered volcanic ash layer (tosteins) in Late Permian coal-bearing formations of eastern Yunnan and western Guizhou Province, China.* International Journal of Coal Geology, 44, 305-324.

Received at: 21. 04. 2017
Accepted for publication at: 30. 06. 2017
Revised at: 22. 06. 2017
Published online at: 18. 07. 2017